Journal of Engineering and Applied Sciences 13 (7): 1877-1887, 2018
ISSN: 1816-949X

Influence of Geometric Error on Accuracy of Industrial Robot

Yeon Taek oh
Department of Mechanical Engineering, Tongmyong University,
428 Sinseon-ro, Nam-gu, Busan, Korea

Abstract: The study proposed a technique to analyse robot's geometric error by using the data measured during circle contouring movement of the industrial robot end effectors. Each joints of the industrial robot must be set at a right angle to be able to move the robot's end effectors to an intended position when an off line program is used. However, the robot joints do not form a precise right angle, the end effectors occurs position error when the robot is under operation. To analyze the angle error of the robot joints (i.e., datum location error), the position measured during circular contouring of the end effectors is used. The shape of the measured circle is also applied to analyze gear transmission error. The study carried out a simulation to find out that datum location error and gear transmission error are the important error factors for accuracy of articulated robots.

Key words: Geometric error, circular contouring, datum location error, gear transmission error, error characteristic, robots

INTRODUCTION

An improved process by robots recently emerged as the way to enhance productivity, competency and quality at a time when many goods are manufactured. Under the circumstance, the industrial robot became a vital factor of the automatic manufacturing line. However, applying it to the actual environment is difficult as it needs new programming for any modification.

The challenge can be resolved with off line programs that would help a robot perform a new task with high position and pose accuracy. Accuracy of the robot should be compensated as well for better use of the off line programs.

When the robot parameter does not coincide with the designer's intention, the error occurs between the taught position and the design data-based position. If the control parameter set up in the initial stage is applied to the robot hardware exactly, the robot system becomes a new one in accuracy perspective. To control the end effectors of an articulated robot to intended locations in general, controller for each driving axis are calculated based on modeling parameter. Therefore, the end effectors deviate from the expect position to have position and pose error when the actual kinematic parameter has error.

There are two ways to address the position error of the robot. One is using the sensor and control technology and the other is calculating the robot parameter through measurement before modifying the control parameter of the controller.

Calibration through direct measurement identifies the error that can occur at the kinematic parameter and includes it in the modeling to eliminate the end effector error. This method is good as it shows the component error directly. However, it is very time consuming as it measures error of the robot joints, links and base and it is also hard to measure the robot joint error once the robot is completely assembled (Oh, 2011a, b).

Kinematic compensation uses the kinematic relationship between the measured position and control position for each driving part using calibration. This method uses modeling that includes each kinematic parameter and error to calculate the measured position that corresponds to the controlling instructions of each driving axis. Then, each position is measured with external measurement device. Then, optimization of minimizing the difference between the calculation value from the modeling and the value from the external measurement tool is done to calculate the kinematic error. As the kinematic calibration can be performed even when the device is under operation, it is useful to calibrate an robot system.

The robot parameter is calibrated to reduce the robot teaching time, failure cost and operating the robot system efficiently as required works are increasingly diverse and complicated. Off line teaching can be done on a separate work area or the computer simulation result can be used for the robot rather instead of direct teaching. In other words, accurate robot system and exact geometric information of the target to work on is enough under off line program to efficiently produce an operation program for multiple robots and this can prevent malfunctioning and conflict during operation of the robot system. However, calibration of inaccurate robot parameters is

needed to apply the off line programming to the industry. The parameters are used to build system model of the robot and work subject on the computer for the off line program and kinematic relationship.

Geometric errors in robots, i.e., errors in joint angles and datum location error are considered to be the main sources of position error (Oh, 2011, 2015). The repeatability errors are non-geometric; these include gear transmission error, joint drive compliance, backlash, bearing and encoder inaccuracy. Other sources of robot inaccuracy include link geometry errors, elastic deflection, scale and control errors and environmental effects. In this study, the effect of geometric errors on the kinematics is theoretically simulated and analysed.

MATERIALS AND METHODS

The influence of datum location errors on robot position: The actual link parameter values for the Fanuc robot on which the tests were conducted were supplied by manufacturer. Theoretically the Fanuc robot is set square in the all axes but in practice the robot axes are not exactly square due to the inaccurate setting. A computer program was developed to carry out the direct kinematic solution which the following conditions were analysed.

For convenient notation, the theta, W, U, gamma, beta and alpha axes of the Fanuc robot are defined θ_1-θ_6. A datum location error of +0.1° is then introduced to θ_1, then θ_1 and θ_2, then θ_1-θ_3 as shown Table 1. In all cases the theoretical end effector positions were calculated for zero error and the introduced error, so, the effect of datum location error could be quantified. The main axes errors are greater than the wrist part axes errors. The angle error of the θ_6 has no relationship with robot position error (Fig. 1).

Position error = Actual position coordinates-desired position coordinates and magnitude $|\bar{e}| = \sqrt{e_x^2 + e_y^2 + e_z^2}$

An error of 0.025°-0.1° was introduced to θ_1-θ_3 while holding θ_4-θ_6 at 0°. Then, θ_1-θ_3 were varied in steps of 5° through the full range of movement. This analysis was further repeated with introduced errors of 0.025°-0.1° in wrist part axes. The computed results show in Fig. 2-6.

The position error of the main axes is shown in Fig. 2-4. The position error is found constant over the range of θ_1 axis in Fig. 2. The position error is shown in Fig. 4 for errors in θ_1-θ_3 of 0.1° over the θ_3 range of -120° to +120°. This position error shows a non linear relationship over the θ_3 range even though the datum

Table 1: Computed position error at datum location error of the robot axes

	Position error (mm)			
Variables	e_x	e_y	e_z	e
Main axes				
0.1° error in θ_1	-0.2238	1.5706	0.0000	1.5865
0.1° error in θ_1, θ_2	0.8189	1.5724	0.0004	1.7729
0.1° error in θ_1, θ_2, θ_3	0.5910	1.5724	1.2206	2.0764
Wrist part axes				
0.1° error in θ_4	0.0000	-0.0002	-0.1745	0.1745
0.1° error in θ_4 θ_5	-0.0002	0.0003	0.0873	0.0873
0.1° error in θ_4 θ_5, θ_6	-0.0002	0.0003	0.0873	0.0873

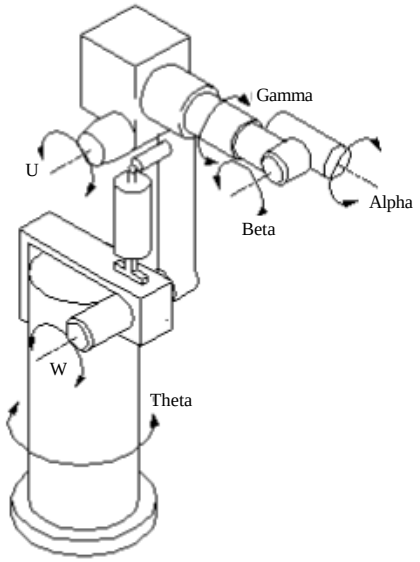

Fig. 1: Link coordination systems for the Fanuc robot

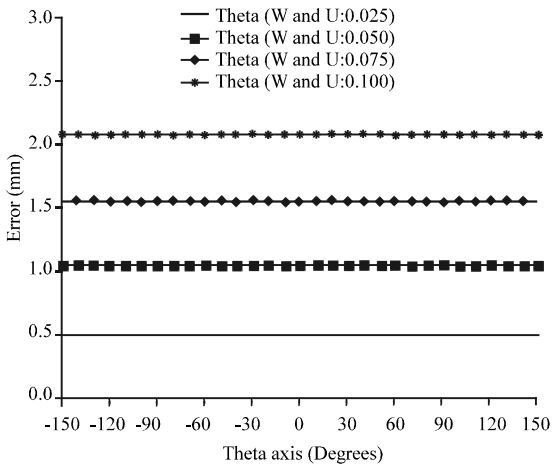

Fig. 2: Theoretical position error in theta axis (θ_1)

location errors are constant. This is due to the changing robot axis position in the robot working space. Therefore, position errors shown for a 0.1° location error the θ_1-θ_3

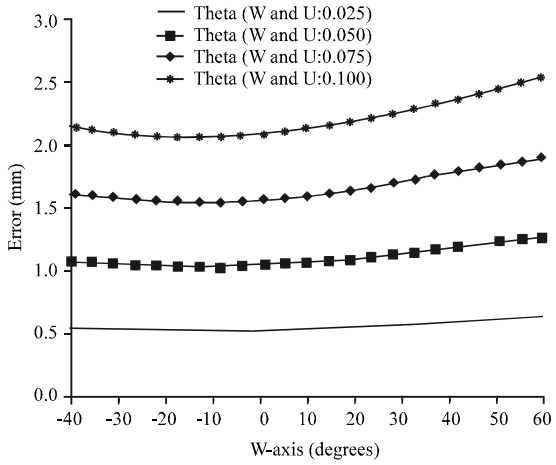

Fig. 3: Theoretical position error in W-axis (θ_2)

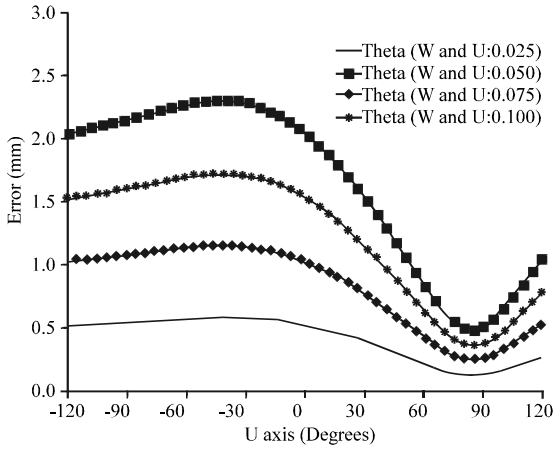

Fig. 4: Theoretical position error in U axis (θ_3)

varies between 0.5-2.3 mm over the θ_3 range in Fig. 4. Also the position error of the wrist axes is shown in Fig. 5 and 6. Compared with the main axes error, the position error of the wrist part in the robot is significantly small. Figure 6 shows the position error over the range of θ_5. The error is symmetrical about the 0° position of the beta axis with a maximum error of 0.44 mm.

Comparing error characteristics between the robot and machine tools: Generally the motion error during circular interpolation is defined by Kakino *et al.* (1987) for NC machine tools. The location of each of the axes of the NC machine is always constant compared to the world coordination system. The possible error origins of NC machine tools have been classified into several groups based on the motion error traces obtained from circular contouring tests. Theoretical analyses were made to determine the characteristic trace patterns.

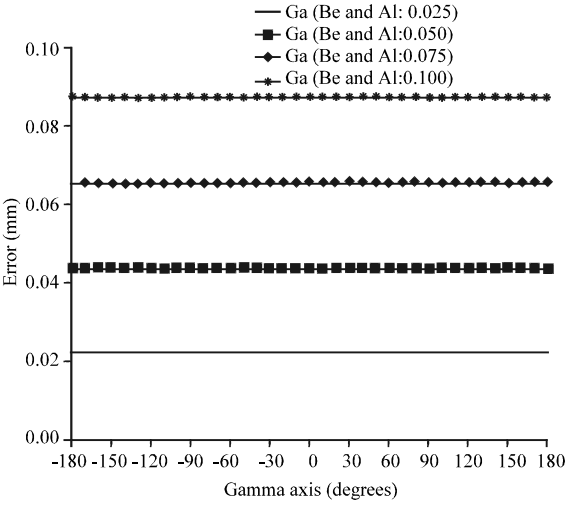

Fig. 5: Theoretical position error in gamma axis (θ_4)

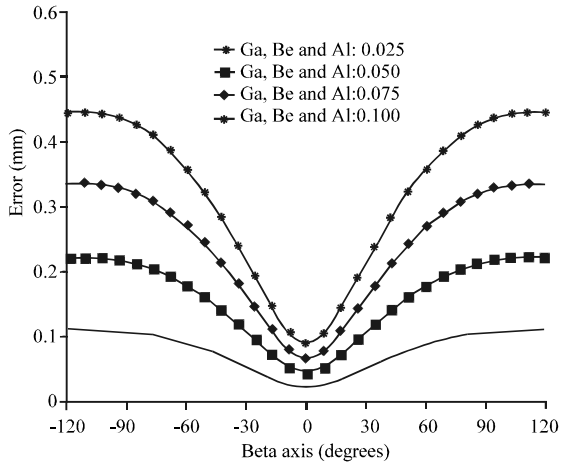

Fig. 6: Theoretical position error in beta axis (θ_5)

These can be extracted from the measured motion error traces for diagnosis of the possible sources of error.

In the case of robots, the location of the axes is changed by the position in the world coordinate system, except for the theta axis which is the fixed axis, i.e., the robot axes positions are moved during the circular contouring and depend on the size and position of the circular path. For example, the backlash in NC machine tools occurs in the X and Y axis during the circular contouring motion in the XY plane. This is usually independent of the circle position and the size of the circle. Also if there is position error in the NC machine tools, this position error will correspond only to the X or y-axis. However, the backlash point in the robot axis can occur at any position during the circular contouring motion which is dependant on the position and the size of the circle. If there is angular error of the robot axis, this

may correspond to a combination of X-Z error in the robot working space. Therefore, the possible error origins in the robot were classified into several groups based on the motion error traces obtained by the circular contouring test and analysed by circle radius which are combinations of X-Z position errors.

RESULTS AND DISCUSSION

The theoretical analyses of the motion errors of the Fanuc robot and the diagnosis of their origins in a 2 axes operation: In order to verify the robot axes error, simulated test data were generated using the direct kinematic solution and analysed by the developed analysis program (Oh, 2011, 2015). Different error values, relating to the datum location and angle error were introduced and compared with the analysed values produced by the analysis program.

Datum location error of the U axis: Circular contouring was generated with the datum location error in the U axis; the resultant plot of the circle is shown in Fig. 7. Figure 7 shows the elliptical shape of the simulated result of circular contouring with ±0.6° datum location error. The circle shapes and least squares circle are different but the error bands are almost the same. Figure 8 shows the correspond linear plot of Fig. 7. The centre line corresponds to the least squares circle whereas the amplitude of the sine wave error is dependant upon the value of the datum location error.

The sine wave curve can be expressed as the fourier series which represents a function of a trigonometrical series of the wave form. The general fourier series representing f(x) can be expressed as

$$f(x)=\frac{1}{2}a_0+a_1\text{Cos}x+a_2\text{Cos}2x+a_3\text{Cos}3x+,\cdots,$$
$$+b_1\text{Sin}x+b_2\text{Sin}2x+b_3\text{Sin}3x+,\cdots$$

where, a_0-a_3, ..., b_1-b_3 are the Fourier coefficients of f(x). x is the angle of the circular contouring. The linear plot of the datum location error of the U axis is expressed as shown in Table 2. Fig. 9 shows the relationship between the datum location error and Fourier coefficients. As shown in Fig. 9, the Fourier coefficient is proportional to the datum location error and this relationship is expresse with a linear function. The datum location error is presented following the general equation:

Table 2: Fourier coefficients of the datum location error

Datum location error (Deg.)	Fourier coefficient					
	a_0	a_1	a_2	a_3	a_4	a_5
-0.6	-0.0015	0.0023	0.7429	-0.0723	-0.0022	0.0055
-0.2	-0.0002	0.0002	0.2475	-0.0242	-0.0009	0.0019
0.2	0.0001	0.0002	-0.2475	0.0242	0.0008	-0.0020
0.6	0.0015	0.0024	-0.7422	0.0724	0.0026	-0.0060
	b_1	b_2	b_3	b_4	b_5	
-0.6	-0.0001	0.7706	-0.1795	-0.0109	-0.0109	
-0.2	-0.0000	0.2569	-0.0600	-0.0037	-0.0037	
0.2	-0.0000	-0.2569	0.0602	0.0038	0.0038	
0.6	-0.0001	-0.7706	0.1811	0.0119	0.0119	

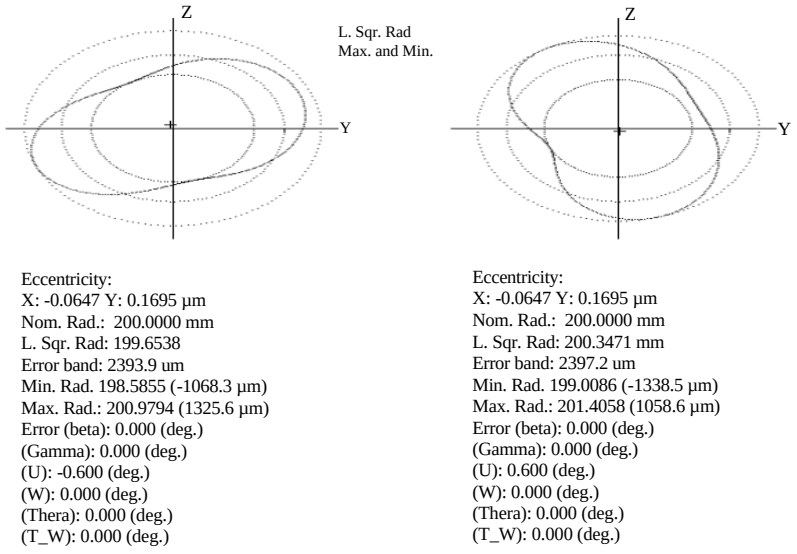

Eccentricity:
X: -0.0647 Y: 0.1695 µm
Nom. Rad.: 200.0000 mm
L. Sqr. Rad: 199.6538
Error band: 2393.9 um
Min. Rad. 198.5855 (-1068.3 µm)
Max. Rad.: 200.9794 (1325.6 µm)
Error (beta): 0.000 (deg.)
(Gamma): 0.000 (deg.)
(U): -0.600 (deg.)
(W): 0.000 (deg.)
(Thera): 0.000 (deg.)
(T_W): 0.000 (deg.)

Eccentricity:
X: -0.0647 Y: 0.1695 µm
Nom. Rad.: 200.0000 mm
L. Sqr. Rad: 200.3471 mm
Error band: 2397.2 um
Min. Rad. 199.0086 (-1338.5 µm)
Max. Rad.: 201.4058 (1058.6 µm)
Error (beta): 0.000 (deg.)
(Gamma): 0.000 (deg.)
(U): 0.600 (deg.)
(W): 0.000 (deg.)
(Thera): 0.000 (deg.)
(T_W): 0.000 (deg.)

Fig. 7: Simulation result of the datum location error of the U-axis

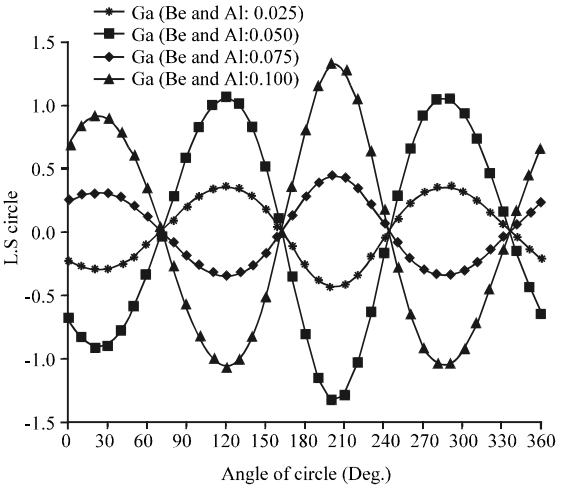

Fig. 8: Linear plot of the datum location error of the U-axis

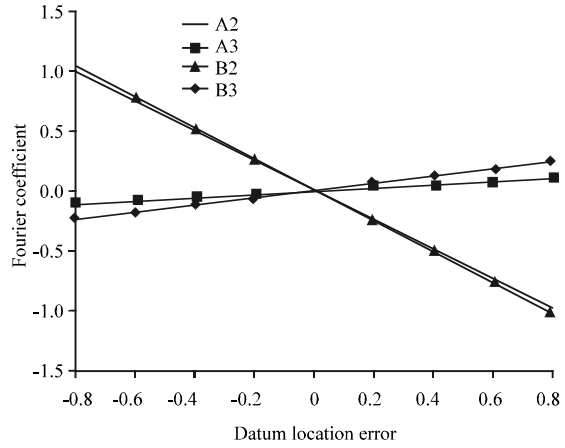

Fig. 9: The relationship between the datum location error and the Fourier coefficient

$$f(x) = (ac_{c0}+d_{c0}) + (ac_{c1}+d_{c1})Cosx + (ac_{c2}+d_{c2})Cos2x + (ac_{c3}+d_{c3})Cos3x + \cdots + (ac_{s1}+d_{s1})Sinx + (ac_{s2}+d_{s2})Sin2x + (ac_{s3}+d_{s3})Sin3x + \cdots$$

where, a_{c0}-a_{c3},..., a_{s1}-a_{s3}, ..., are the slopes of the coefficients and d_{c0}, d_{c1}, d_{c2}, d_{c3},..., d_{s1}, d_{s2}, d_{s3}, ..., are the intersection of the axis in the linear function.

These coefficients of the fourier series are shown in the Table 3. In the general equation a is the datum location error of the U axis. The datum location error (a) is found using the least square approximation in the Fourier series.

Table 3: The coefficient of the linear equation of the fourier series

Slope of the linear function					
a_{c0}	a_{c1}	a_{c2}	a_{c3}	a_{c4}	a_{c5}
-0.00001	0.00002	-1.23766	0.12116	0.00396	-0.00963
Slope of the linear function (a_1):					
a_{s1}	a_{s2}	a_{s3}	a_{s4}	a_{s5}	
0.00003	-1.28433	0.30049	0.01894	0.01894	
Intersection of the y-axis in the linear slope:					
d_{c0}	d_{c1}	d_{c2}	d_{c3}	d_{c4}	d_{c5}
-0.00126	0.00198	0.00030	-0.00025	0.00014	-0.00021
Intersection of the y-axis in the linear slope (d_1):					
d_{s1}	d_{s2}	d_{s3}	d_{s4}	d_{s5}	
-0.00007	0.00003	0.00067	0.00042	0.00042	

Datum location error of the W axis: The angle motion of the robot joint is achieved by the use of a motor and reduction gearing mechanism, i.e., 'Cyclo' type reduction gear or harmonic drive etc. Therefore the main error source of the robot joint error comes from the eccentricity between the centre of the motor and reduction gearing mechanism (Oh, 2011). The characteristic of gear transmission error is expressed as a sine function in the robot axes. Fig. 10 shows the resultant plot with $\pm 0.06\text{Sin}\theta$ angular error of the robot W axis. The error bands are similar but the least squares circle and the contouring shapes are different. Figure 11 shows the corresponding linear plot of Fig. 10. The centre line corresponds to the least squares circle. The null point always occurs at the same position in Fig. 11. It indicates that the null points are independent of the gear transmission error whereas the amplitude of the sine wave is dependant only on the gear transmission error. Therefore the sine wave error can be represented as the fourier series (Lie *et al*., 2004).

$$f(x) = (ac_{c0}+d_{c0}) + (ac_{c1}+d_{c1})Cosx + (ac_{c2}+d_{c2})Cos2x + (ac_{c3}+d_{c3})Cos3x + +, \cdots, + (ac_{s1}+d_{s1})Sinx + (ac_{s2}+d_{s2})Sin2x + (ac_{s3}+d_{s3})Sin3x + , \cdots,$$

These coefficients of the Fourier series are shown in the Table 3. Where a is the gear transmission error of the W axis.

Datum location error of the U axis: The characteristics of the U axis gear transmission error are shown in Fig. 12. These are similar to the error form of the W axis gear transmission. Only variations in the null points and amplitude occur in the linear plot between Fig. 13 and 11; the form remains the same. Therefore the sine wave form can also be expressed as a Fourier series. Table 4 and 5 shows the coefficients of the this series (Chen *et al*., 2008).

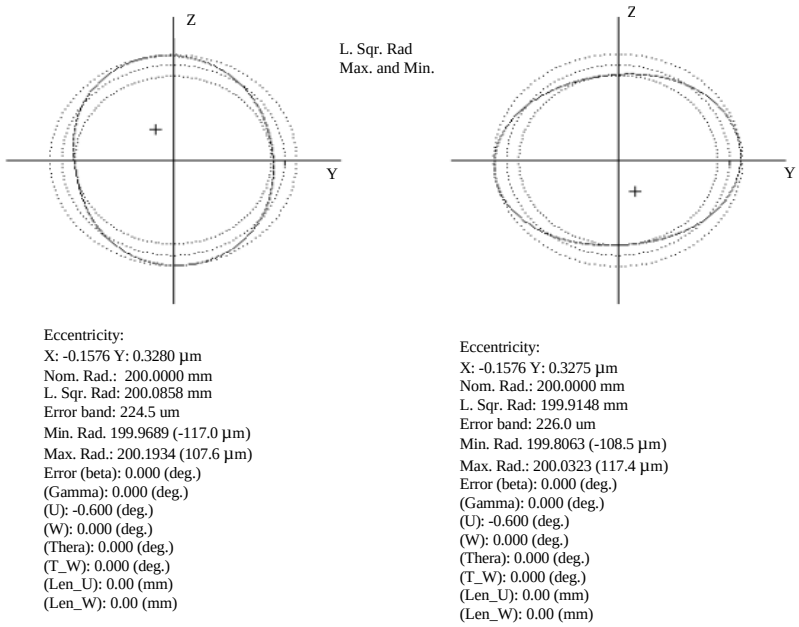

Fig. 10: Simulation result of the gear transmission error of the W axis

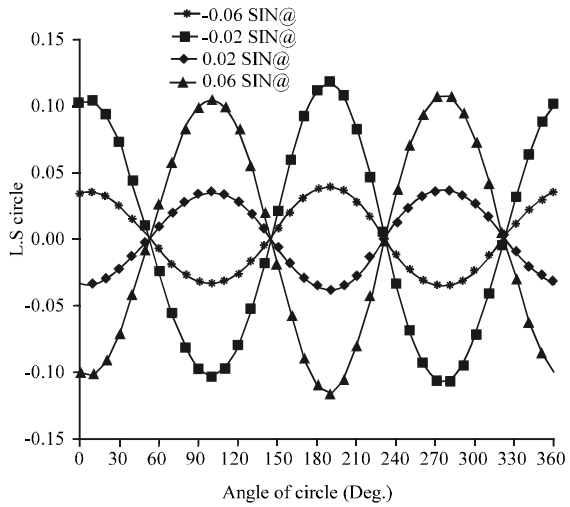

Fig. 11: Linear plot of the gear transmission error of the W-axis

$$f(x) = (ac_{c0}+d_{c0})+(ac_{c1}+d_{c1})Cosx$$
$$+(ac_{c2}+d_{c2})Cos2x+(ac_{c3}+d_{c3})Cos3x$$
$$+,\cdots,+(ac_{s1}+d_{s1})Sinx+(ac_{s2}+d_{s2})Sin2x$$
$$+(ac_{s3}+d_{s3})Sin3x+,\cdots,$$

Datum location error of the Beta axis: Figure 14 shows the resultant plot with ±0.6° datum location error in the beta axis. The error configuration is shown in Fig. 16. The resultant plot of the circular contouring has an elliptical shape. Figure 15 shows the corresponding linear plot of Fig. 14. The null points are independent of the datum location error and therefore the this form can be expressed as a Fourier series. Table 6 presents the coefficients of the Fourier series.

Table 4: The coefficient of the linear equation of the Fourier series

Slope of the linear function					
a_{c0}	a_{c1}	a_{c2}	a_{c3}	a_{c4}	a_{c5}
-0.00005	0.00000	1.73428	-0.07945	0.03387	-0.00544
Slope of the linear function (a_1):					
a_{s1}	a_{s2}	a_{s3}	a_{s4}	a_{s5}	
0.00003	0.46464	-0.07783	-0.00861	-0.00861	
Intersection of the y-axis in the linear slope:					
d_{c0}	d_{c1}	d_{c2}	d_{c3}	d_{c4}	d_{c5}
0.00000	-0.00002	0.00017	0.00005	-0.00001	0.00000
Intersection of the y-axis in the linear slope (d_1):					
d_{s1}	d_{s2}	d_{s3}	d_{s4}	d_{s5}	
0.00001	0.00021	-0.00007	0.00000	0.00000	

Table 5: The coefficient of the linear equation of the fourier series

Slope of the linear function					
a_{c0}	a_{c1}	a_{c2}	a_{c3}	a_{c4}	a_{c5}
-0.00017	0.00000	-0.33329	0.16359	-0.08768	0.03463
Slope of the linear function (a_1):					
a_{s1}	a_{s2}	a_{s3}	a_{s4}	a_{s5}	
0.00000	1.61448	-0.42019	-0.01774	-0.01774	
Intersection of the y-axis in the linear slope:					
d_{c0}	d_{c1}	d_{c2}	d_{c3}	d_{c4}	d_{c5}
0.00002	-0.00015	0.00006	-0.00005	0.00002	-0.00000
Intersection of the y-axis in the linear slope (d_1):					
d_{s1}	d_{s2}	d_{s3}	d_{s4}	d_{s5}	
0.00010	-0.00014	0.00001	0.00000	0.00000	

Datum location error of the gamma axis: The characteristics of the datum location error of the Gamma

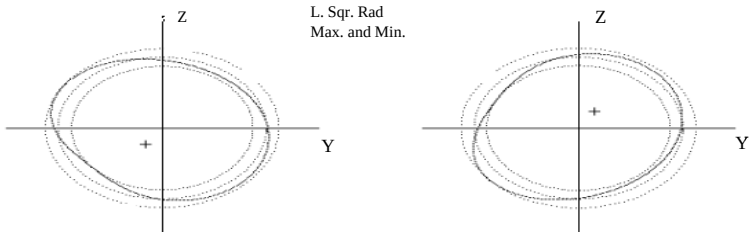

Eccentricity:
X: -0.1551 Y: -0.2338 µm
Nom. Rad.: 200.0000 mm
L. Sqr. Rad: 199.9362 mm
Error band: 248.2 um
Min. Rad. 199.8075 (-128.7 µm)
Max. Rad.: 200.0558 (119.6 µm)
Error (beta): 0.000 (deg.)
(Gamma): 0.000 (deg.)
(U): -0.600 (deg.)
(W): 0.000 (deg.)
(Thera): 0.000 (deg.)
(T_W): 0.000 (deg.)
(Len_U): 0.00 (mm)
(Len_W): 0.00 (mm)

Eccentricity:
X: 0.1555 Y: 0.2342 µm
Nom. Rad.: 200.0000 mm
L. Sqr. Rad: 200.0643 mm
Error band: 247.1 um
Min. Rad. 199.9448 (-199.4 µm)
Max. Rad.: 200.1919 (127.6 µm)
Error (beta): 0.000 (deg.)
(Gamma): 0.000 (deg.)
(U): -0.600 (deg.)
(W): 0.000 (deg.)
(Thera): 0.000 (deg.)
(T_W): 0.000 (deg.)
(Len_U): 0.00 (mm)
(Len_W): 0.00 (mm)

Fig. 12: Simulation result of the gear transmition error of the U axis

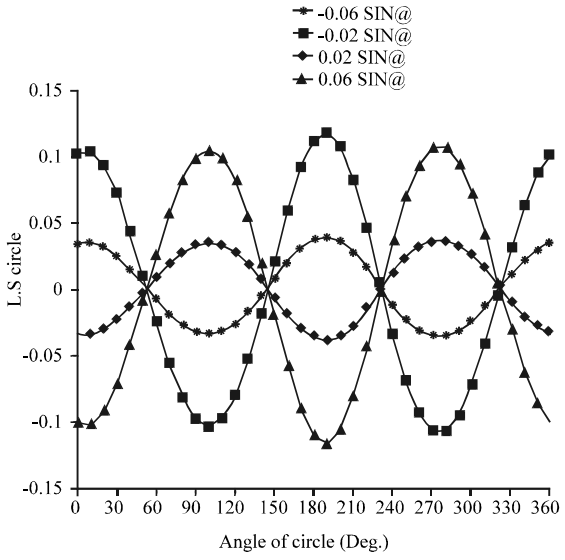

Fig. 13: Linear plot of the gear transmission error of the U-axis

$$f(x) = (ac_{c0} + d_{c0}) + (ac_{c1} + d_{c1})Cosx$$
$$+(ac_{c2} + d_{c2})Cos2x + (ac_{c3} + d_{c3})Cos3x + \cdots,$$
$$+(ac_{s1} + d_{s1})Sinx + (ac_{s2} + d_{s2})Sin2x +$$
$$(ac_{s3} + d_{s3})Sin3x + \cdots,$$

axis also show a similar tendency to that mentioned in the previous sections. The error configuration is shown in Fig. 16. Figure 16 shows the resultant plot of the circular contouring with ±0.6° datum location error of the Gamma axis with the corresponding linear plot shown in Fig. 17 This form can again be expressed as a fourier series equation with the corresponding coefficient given in Table 7.

Table 6: The coefficient of the linear equation of the fourier series

Slope of the linear function

a_{c0}	a_{c1}	a_{c2}	a_{c3}	a_{c4}	a_{c5}
-0.00006	0.00000	0.33748	-0.08205	0.02308	-0.00536

Slope of the linear function (a_1):

a_{s1}	a_{s2}	a_{s3}	a_{s4}	a_{s5}
0.00000	-0.36054	0.03779	-0.00240	-0.00240

Intersection of the y-axis in the linear slope:

d_{c0}	d_{c1}	d_{c2}	d_{c3}	d_{c4}	d_{c5}
-0.00007	0.00011	-0.00011	0.00002	0.00002	0.0000

1Intersection of the y-axis in the linear slope (d_1):

d_{s1}	d_{s2}	d_{s3}	d_{s4}	d_{s5}
0.00012	-0.00009	0.00008	-0.00003	-0.00003

Table 7: The coefficient of the linear equation of the fourier series

Slope of the linear function

a_{c0}	a_{c1}	a_{c2}	a_{c3}	a_{c4}	a_{c5}
0.00000	0.00000	0.35595	-0.03752	0.00017	0.00233

Slope of the linear function (a_1):

a_{s1}	a_{s2}	a_{s3}	a_{s4}	a_{s5}
0.00000	0.33059	-0.07989	-0.00530	-0.00530

Intersection of the y-axis in the linear slope:

d_{c0}	d_{c1}	d_{c2}	d_{c3}	d_{c4}	d_{c5}
-0.00009	0.00014	-0.00083	0.00010	-0.00001	0.00001

Intersection of the y-axis in the linear slope (d_{s1}):

d_{s1}	d_{s2}	d_{s3}	d_{s4}	d_{s5}
0.00000	-0.00032	0.00016	0.00004	0.00004

Error analysis with simulated contouring: In order to analyse the circular contouring, simulated test data were

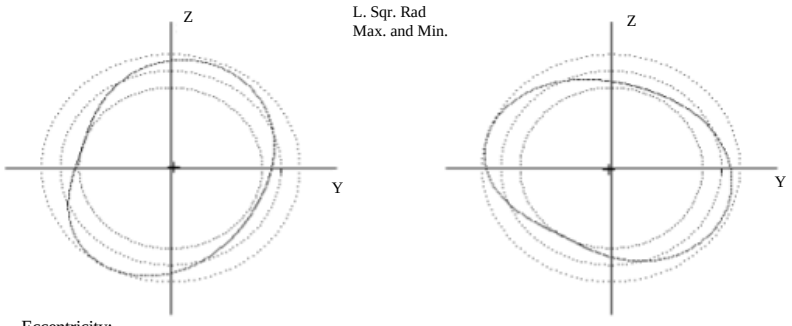

Eccentricity:
X: 0.0526 Y: 0.0241 µm
Nom. Rad.: 200.0000 mm
L. Sqr. Rad: 200.2799 mm
Error band: 683.6 um
Min. Rad. 199.9392 (-340.7 µm)
Max. Rad.: 200.6228 (342.9 µm)
Error (beta): 0.000 (deg.)
(Gamma): 0.000 (deg.)
(U): -0.600 (deg.)
(W): 0.000 (deg.)
(Thera): 0.000 (deg.)
(T_W): 0.000 (deg.)
(Len_U): 0.00 (mm)
(Len_W): 0.00 (mm)

Eccentricity:
X: 0.0524 Y: 0.0236 µm
Nom. Rad.: 200.0000 mm
L. Sqr. Rad: 199.7207 mm
Error band: 683.9 um
Min. Rad. 199.3768 (-343.9 µm)
Max. Rad.: 200.0608 (340.1 µm)
Error (beta): 0.600 (deg.)
(Gamma): 0.000 (deg.)
(U): -0.600 (deg.)
(W): 0.000 (deg.)
(Thera): 0.000 (deg.)
(T_W): 0.000 (deg.)
(Len_U): 0.00 (mm)
(Len_W): 0.00 (mm)

Fig. 14: Simulation result of the gear transmission error of the Beta axis

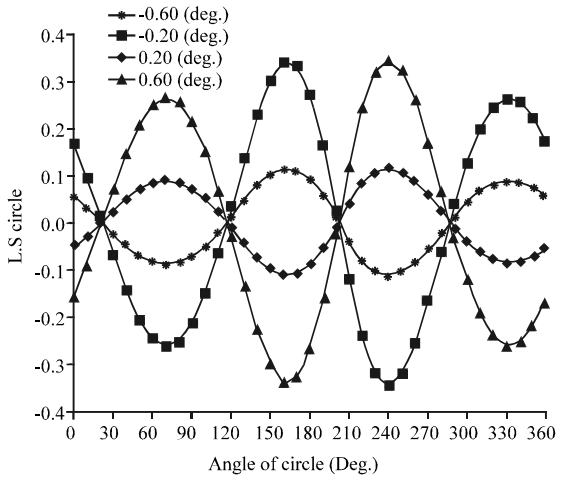

Fig. 15: Linear plot of the gear transmission error of the Beta axis

generated and analysed using the developed analysis program based on the fourier series equations. Different error values, relating to the gear transmission error of the U and W-axes and the datum location error of the beta, gamma and U-axes were introduced and compared with the analysed value from the analysis program. Some examples of the simulation of contouring test data and analysis are given.

Table 8 gives the error values used to generate synthetic data to test the analysis software. Then test result in the circular contouring test is plotted in Fig. 18. Table 9 gives the error values used to generate synthetic data to test the analysis software.

Then test result in the circular contouring test is plotted as in the Fig. 19. If the robot errors during the circular contouring test in the 2 robot axes operation are: then test result in the circular contouring test is plotted as in Fig. 9-20.

Table 8: The error values used to generate synthetic data to test the analysis software

Variables	Values
Dattum location error of the Beta axis (deg.)	0
Datum location error of the gamma axis (deg.)	0
Datum location error of the U axis (deg.)	0
Gear transmission error of the U axis (deg.)	0
Gear transmission error of the W axis (deg.)	0

Table 9: The error values used to generate synthetic data to test the analysis software

Variables	Values
Datum location error of the Beta axis (deg.)	0.2
Datum location error of the gamma axis (deg.)	0.2
Datum location error of the U axis (deg.)	0.2
Gear transmission error of the U axis (deg.)	0.0
Gear transmission error of the W axis (deg.)	0.0

Table 10: If the robot errors during the circular contouring test in the 2 robot axes operation

Variables	Values
Datum location error of the beta axis (deg.)	0.2
Datum location error of the gamma axis (deg.)	0.2
Datum location error of the U axis (deg.)	0.2
Gear transmission error of the U axis (deg.)	0.2sinθ
Gear transmission error of the W axis (deg.)	0.2Sinθ

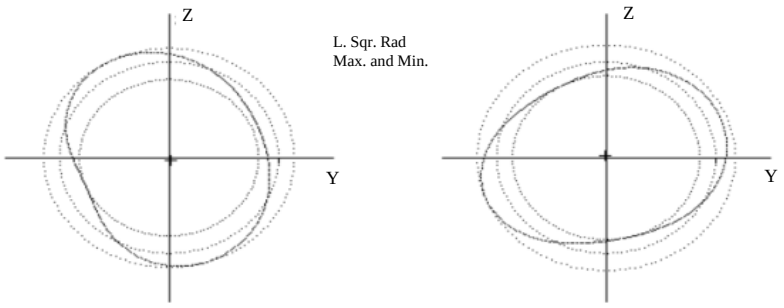

Eccentricity:
X: 0.0211 Y: 0.0450 µm
Nom. Rad.: 200.0000 mm
L. Sqr. Rad: 200.1133 mm
Error band: 654.6 um
Min. Rad. 199.7488 (-340.7 µm)
Max. Rad.: 200.4035 (342.9 µm)
Error (beta): 0.000 (deg.)
(Gamma): -0.600 (deg.)
(U): -0.600 (deg.)
(W): 0.000 (deg.)
(Thera): 0.000 (deg.)
(T_W): 0.000 (deg.)
(Len_U): 0.00 (mm)
(Len_W): 0.00 (mm)

Eccentricity:
X: 0.0206 Y: 0.0447 µm
Nom. Rad.: 200.0000 mm
L. Sqr. Rad: 199.8938 mm
Error band: 649.3 um
Min. Rad. 199.6055 (-288.3 µm)
Max. Rad.: 200.2548 (361.0 µm)
Error (beta): 0.000 (deg.)
(Gamma): 0.600 (deg.)
(U): 0.000 (deg.)
(W): 0.000 (deg.)
(Thera): 0.000 (deg.)
(T_W): 0.000 (deg.)
(Len_U): 0.00 (mm)
(Len_W): 0.00 (mm)

Fig. 16: Simulation result of the gear transmission error of the gamma axis

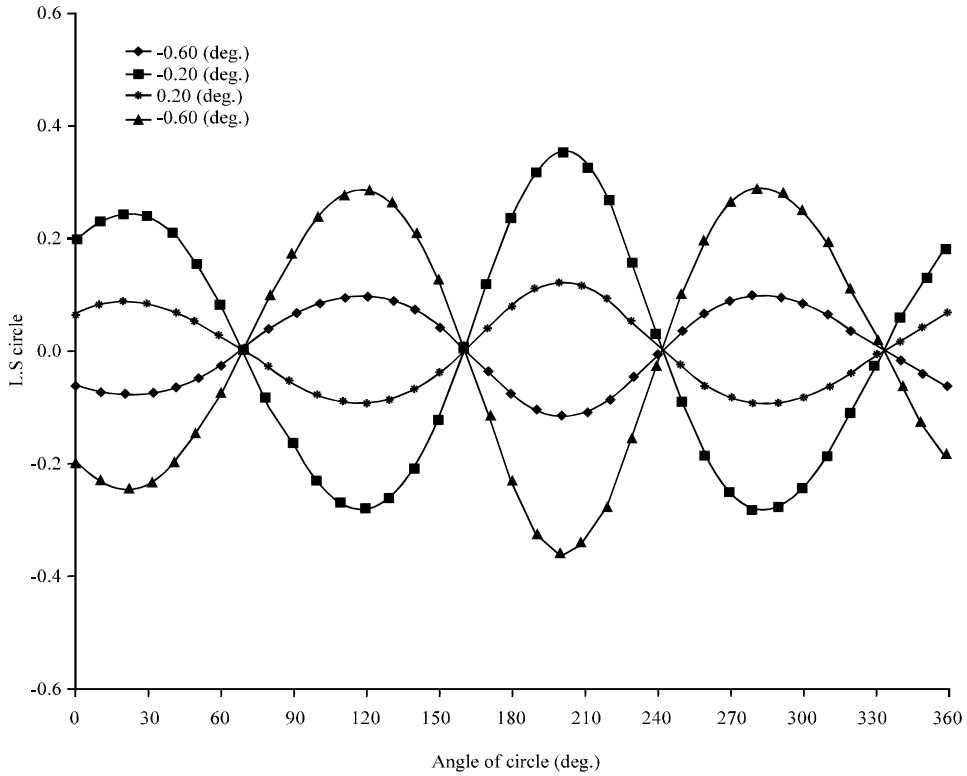

Fig. 17: Linear plot of the gear transmission error of the gamma axis

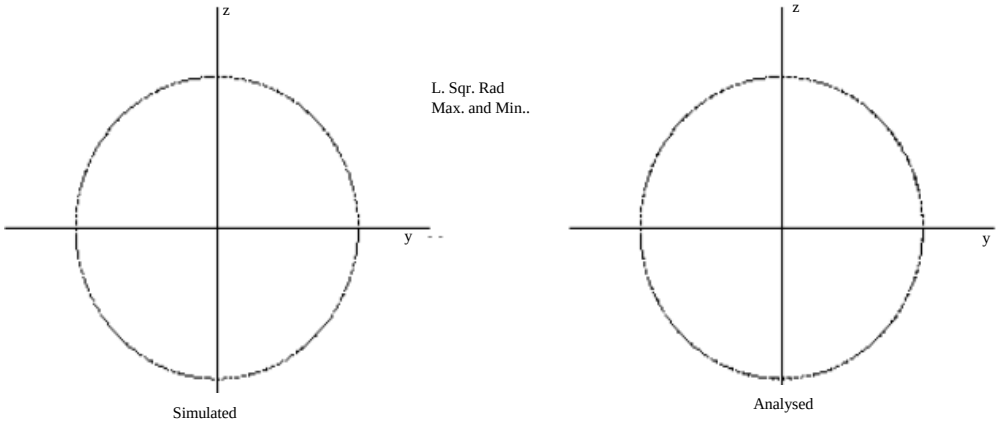

Simulated

Nom. Rad.: 200.0000 mm
L. Sqr. Rad: 200.0000 mm
Error band: 0.0 um
Min. Rad. 200.0000 (-0.0 µm)
Max. Rad.: 200.0000 (0.0 µm)
Error (beta): 0.000 (deg.)
(Gamma): 0.000 (deg.)
Angle (U): 0.000 (deg.)
(Angle of U: 0.000*sin θ (deg.)
Angle of M: 0.000*sinθ (deg.)

Analysed

Nom. Rad.: 200.0000 mm
L. Sqr. Rad: 199.9994 mm
Error band: 3.8 um
Min. Rad. 199.9976 (-1.8 µm)
Max. Rad.: 200.00140 (2.0 µm)
Error (beta): 0.001 (deg.)
(Gamma): 0.002 (deg.)
(U): 0.001 (deg.)
(Angle of U: 0.001*sin θ (deg.)
Angle of M: 0.001*sinθ (deg.)

Fig. 18: The comparison between the given and analysed data 1

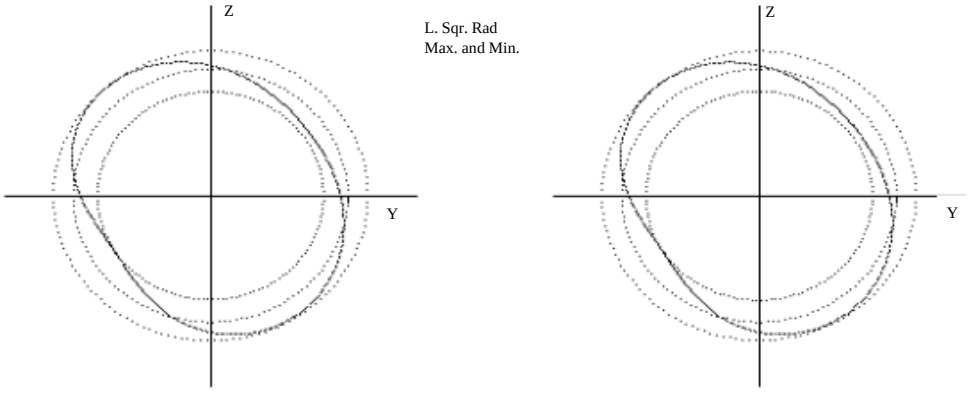

Simulated

Nom. Rad.: 200.0000 mm
L. Sqr. Rad: 199.9861 mm
Error band: 645.0 um
Min. Rad. 199.6333 (-352.8 µm)
Max. Rad.: 200.2783 (292.2 µm)
Error (beta): 0.200 (deg.)
(Gamma): 0.200 (deg.)
(U): 0.300 (deg.)
(Angle of U: 0.000*sin θ (deg.)
Angle of M: 0.000*sinθ (deg.)

Analysed

Nom. Rad.: 200.0000 mm
L. Sqr. Rad: 199.9835 mm
Error band: 635.1 um
Min. Rad. 199.6360 (-347.5 µm)
Max. Rad.: 200.2783 (287.6 µm)
Error (beta): 200.2711 (287.6 µm)
(Gamma): 0.202 (deg.)
(U): 0.199 (deg.)
(Angle of U: 0.000*sin θ (deg.)
Angle of M: 0.000*sinθ (deg.)

Fig. 19: The comparison between the given and analysed data 2

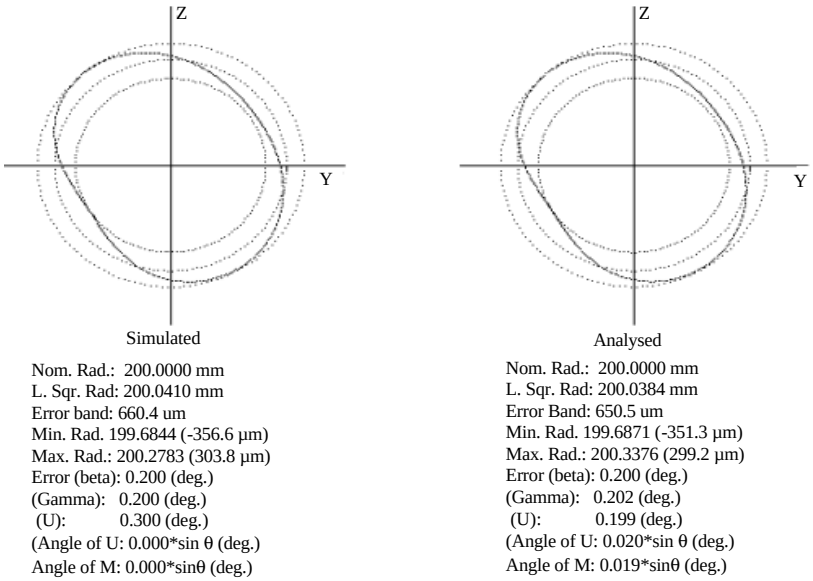

Fig. 20: The comparison between the given and analysed data 3

CONCLUSION

The datum location error was shown to be a significant factor influencing the accuracy of the robot end effector. The test strategy devised using error band data from the circular test, enabled the optimum position of the datum to be established. The technique devised using a simulation program for the robot geometry, together with results from a circular test, enabled the robot error to be characterised in terms of datum location error, backlash, gear transmission error, link length error, axes misalignments, joint encoder offset, closing error and servo mismatch error.

ACKNOWLEDGEMENT

This research was supported by the Tongmyong University Research Grants 2015.

REFERENCES

Chen, H., T. Fuhlbrigge, S. Choi, J. Wang and X. Li, 2008. Practical industrial robot zero offset calibration. Proceedings of the IEEE International Conference on Automation Science and Engineering (CASE 2008), August 23-26, 2008, IEEE, Arlington, Virginia, USA., ISBN:978-1-4244-2022-3, pp: 516-521.

Kakino, Y., Y. Ihara, Y. Nakatsu and K. Okamura, 1987. The measurement of motion errors of NC machine tools and diagnosis of their origins by using telescoping magnetic ball bar method. CIRP. Ann. Manuf. Technol., 36: 377-380.

Lei, S., L. Jingtai, S. Weiwei, W. Shuihua and H. Xingbo, 2004. Geometry-based robot calibration method. Proceedings of the 2004 IEEE International Conference on Robotics and Automation (ICRA'04) Vol. 2, April 26-May 1, 2004, IEEE, New Orleans, Louisiana, USA, ISBN:0-7803-8232-3, pp: 1907-1912.

Oh, Y.T., 2011b. Influence of the joint angular characteristics on the accuracy of industrial robots. Ind. Robot Intl. J., 38: 406-418.

Oh, Y.T., 2011a. Robot accuracy evaluation using a ball-bar link system. Robotica, 29: 917-927.

Oh, Y.T., 2015. Study of datum location error on the accuracy of industrial robot. Intl. J. Eng. Technol., 7: 883-893.